

## $(K^-, K^+)$ reaction on nuclear targets at $P_{K^-} = 1.65 \text{ GeV}/c$

T. Iijima<sup>a</sup>, H. Funahashi<sup>a</sup>, S. Hirata<sup>a,1</sup>, M. Ieiri<sup>b</sup>, K. Imai<sup>a</sup>,  
T. Ishigami<sup>c</sup>, Y. Itow<sup>a</sup>, K. Kikuchi<sup>d</sup>, M. Kobayashi<sup>c</sup>, A. Masaie<sup>a</sup>,  
Y. Matsuda<sup>c</sup>, C. Nagoshi<sup>f</sup>, M. Nakamura<sup>e</sup>, S. Nakanishi<sup>e</sup>, T. Nakano<sup>a,2</sup>,  
H. Shibuya<sup>c</sup>, H.M. Shimizu<sup>a</sup>, H. Tajima<sup>e,3</sup>, R. Takashima<sup>h</sup>,  
F. Takeutchi<sup>i</sup> and H. Togawa<sup>a,4</sup>

<sup>a</sup> Department of Physics, Kyoto University, Kyoto 606, Japan

<sup>b</sup> National Laboratory for High Energy Physics, Tsukuba 305, Japan

<sup>c</sup> Department of Physics, Toho University, Funabashi 274, Japan

<sup>d</sup> Faculty of Education, Utsunomiya University, Utsunomiya 350, Japan

<sup>e</sup> Kobe University, Kobe 657, Japan

<sup>f</sup> Institute for Nuclear Study, University of Tokyo, Tanashi, Tokyo 188, Japan

<sup>g</sup> Department of Physics, Nagoya University, Nagoya 464, Japan

<sup>h</sup> Kyoto University of Education, Kyoto 612, Japan

<sup>i</sup> Kyoto Sangyo University, Kyoto 603, Japan

Received 16 March 1992

**Abstract:** The forward-angle cross sections of the  $(K^-, K^+)$  reaction on nuclear targets of C, Al, Cu, Ag and Pb have been measured at the  $K^-$  incident momentum of  $1.65 \text{ GeV}/c$  in a wide range of  $K^+$  momentum. The obtained  $K^+$  momentum spectrum for each target nucleus is characterized by a peak in the high-momentum region ( $p_{K^+} > 0.95 \text{ GeV}/c$ ) and a broad bump in the low-momentum region ( $p_{K^+} < 0.95 \text{ GeV}/c$ ). A comparison of the measured spectrum with a DWIA calculation indicates that the quasifree process,  $K^-(p) \rightarrow K^+ \Xi^-$ , is dominant in the high-momentum region. The target mass-number dependence of the cross section is well fitted with  $A^\alpha$ , where  $\alpha$  is  $0.38 \pm 0.03$  for the high-momentum region and  $0.56 \pm 0.02$  for the low-momentum region. The result indicates that the quasifree process takes place at the peripheral of the target nucleus, whereas the two-step processes are dominant in the low-momentum region.

E

NUCLEAR REACTIONS p, C, Al, Cu, Ag, Pb ( $K^-, K^+$ ),  $E$  at  $1.65 \text{ GeV}/c$ , measured  $\sigma$  averaged between  $\theta = 1.7^\circ$  and  $13.6^\circ$ , Natural targets.

### 1. Introduction

The  $(K^-, K^+)$  reaction is quite unique, as it is an exchange reaction of two units of both charge and strangeness. Since this reaction provokes a transfer of two

Correspondence to: Dr. K. Imai, Department of Physics, Kyoto University, Kyoto 606, Japan.

<sup>1</sup> Present address: Research Center for Nuclear Physics, Osaka University, Osaka 569, Japan.

<sup>2</sup> Present address: Center for Subatomic Research, Department of Physics, University of Alberta, Edmonton, T6G 2N5, Canada.

<sup>3</sup> Present address: University of California at Santa Barbara, Santa Barbara, California 93106, USA.

<sup>4</sup> Present address: Research Center for Nuclear Physics, Osaka University, Osaka 567, Japan.

strangeness quantum numbers ( $S$ ), it has been trusted to be one of the most promising ways of studying the  $S = -2$  systems such as the H-particle, double hypernuclei and  $\Xi^-$  hypernuclei. Several ways of approaching these objects with the ( $K^-$ ,  $K^+$ ) reaction have been demonstrated in both theoretical and experimental literature. One of the proposed methods is producing these objects with the atomic capture of  $\Xi^-$  created in free space with the ( $K^-$ ,  $K^+$ ) reaction<sup>1,2</sup>). In a recent study of  $\Xi^-$  capture events in emulsion (KEK-E176), evidence of the weak decay of double hypernuclei was found<sup>3,4</sup>). In this experiment, a  $\Xi^-$  was created with the ( $K^-$ ,  $K^+$ ) reaction on an emulsion nucleus such as C, N, O, Ag and Br, then slowed down and captured at rest. Another proposed approach is the direct production of the  $S = -2$  objects by the ( $K^-$ ,  $K^+$ ) reaction on nuclear targets. The H-particle can be directly produced by the process,  $K^-(pp) \rightarrow K^+H$ , where (pp) is a proton pair in a nucleus<sup>5</sup>). In the E176 experiment, upper limits for the H-particle production on the emulsion target was set in the mass range of 1.90–2.16 GeV/ $c^2$  by a careful study of the  $K^+$  momentum spectrum<sup>7</sup>). The coherent production of the  $\Xi^-$  hypernuclei was also discussed in ref.<sup>6</sup>). The ( $K^-$ ,  $K^+$ ) reaction on nuclear targets is of considerable interest in these points of view, however, our knowledge for the ( $K^-$ ,  $K^+$ ) reaction is very limited. Although the cross section has been measured for proton target at various energies<sup>8</sup>) and for deuteron target at  $p_K = 1.4$  GeV/ $c$  [ref.<sup>9</sup>], so far no data have been available on the cross section with nuclear targets. The reaction mechanism is, therefore, unknown for the ( $K^-$ ,  $K^+$ ) reaction on nuclear targets.

According to measurement in the past, the forward-angle cross section of the elementary process,  $K^-p \rightarrow K^+\Xi^-$ , peaks at around  $p_{K^-} = 1.8$  GeV/ $c$  [ref.<sup>5</sup>]. In this energy region, the ( $K^-$ ,  $K^+$ ) reaction can take place by the quasifree one-step process,  $K^-(p) \rightarrow K^+\Xi^-$  or  $K^-(p) \rightarrow K^+\Xi^{*-}(1530)$ , where (p) is a proton in a nucleus. The quasifree process with three particles in the final state,  $K^-(p) \rightarrow K^+\Xi^-\pi^0$  or  $K^-(p) \rightarrow K^+\Xi^0\pi^-$ , is also possible. In the quasifree processes, the distortion effect of the incoming  $K^-$  and the outgoing  $K^+$  is responsible for the cross section. The distortion effect has been discussed in the study of the production of  $\Lambda$ -hypernuclei through single-strangeness exchange reactions such as ( $K^-$  in flight,  $\pi^-$ ), ( $K^-$  at rest,  $\pi^-$ ) and ( $\pi^+$ ,  $K^+$ ) reactions. In theoretical calculations, the distorted-wave impulse approximation (DWIA) has been used to include the distortion effect of the mesons. Bertini *et al.*, for example, measured the forward-angle cross sections of  $A(K^-, \pi^-)_\Lambda$  reaction at  $p_{K^-} = 720$  MeV/ $c$  in a wide range of target mass number<sup>10</sup>). The agreement between the data and the DWIA calculation by Bouyssy<sup>11,12</sup>) assuming only single-neutron process is relatively good, although the calculated cross section is larger than the measured one, especially for heavy nuclei ( $A \geq 40$ ). In the ( $K^-$ ,  $\pi^-$ ) reaction at this energy region, low-lying states of the  $\Lambda$ -hypernuclei are preferentially produced because of the small momentum transfer. In contrast, the ( $K^-$ ,  $K^+$ ) reaction is characterized by the large momentum transfer. For example, the momentum transfer of the  $K^-p \rightarrow K^+\Xi^-$  reaction at  $p_{K^-} = 1.65$  GeV/ $c$  is

0.51 GeV/c even at  $\theta = 0^\circ$ , and it is twice as large as the Fermi momentum. The modification of the quasifree process due to the coherent effect is, therefore, expected to be small.

In second order, the two units of charge and strangeness are transferred through two-nucleon processes. The second-order process was discussed by Dover *et al.* in connection with the production of  $\Lambda\Lambda$  hypernuclei through the two-step strangeness and charge exchange reaction with an intermediate  $\pi^0$ , namely  $K^-(p) \rightarrow \pi^0\Lambda$  followed by  $\pi^0(p) \rightarrow K^+\Lambda$  [refs. <sup>13,14</sup>]. Concerning the double charge exchange reactions (DCX), many experimental and theoretical efforts have been made to study the  $(\pi^-, \pi^+)$  and  $(\pi^+, \pi^-)$  reactions. The DCX is characterized by the fact that at least two nucleons must participate in the reaction to conserve charge in the low-energy region below the quasifree  $\Delta$ -production threshold. In the simplest model, the DCX proceeds through two successive single-charge exchange reactions (SCX) with an intermediate  $\pi^0$ , which take place only on one species of nucleons. In the  $(\pi^-, \pi^+)$  process, for example, the two SCX reactions proceed only on the protons. Taking the strong isospin dependence of the  $\pi N$  interaction into account, Gram *et al.* claimed that this model reproduces well the target mass-number dependence ( $A$ -dependence) of inclusive  $(\pi^-, \pi^+)$  and  $(\pi^+, \pi^-)$  reactions at incident pion energies of 180 and 240 MeV [ref. <sup>15</sup>].

The measurement of the cross section for the  $(K^-, K^+)$  reaction on nuclear targets has, therefore, been awaited for the study of the reaction mechanism of the double charge and strangeness exchange reaction. It will enable us to make more quantitative discussions for the research of the  $S = -2$  systems using the  $(K^-, K^+)$  reaction. In this paper, we present the results of an experiment to measure the forward-angle cross sections of  $(K^-, K^+)$  reaction on C, Al, Cu, Ag and Pb targets at the incident  $K^-$  momentum of 1.65 GeV/c. The experiment was performed at KEK-PS, using a  $K^+$  spectrometer constructed for the emulsion-counter hybrid experiment (E176). This spectrometer has a large momentum acceptance for the outgoing  $K^+$ . The reaction mechanism of the  $(K^-, K^+)$  reaction can be studied with the gross structure of the  $K^+$  momentum spectrum. The measurement in a wide range of the target mass number is advantageous to extract a simple geometrical description of the reaction mechanism.

Sects. 2 and 3 provide a brief description of, respectively, the experiment itself and the data reduction. The results of the experiment are shown in sect. 4. The momentum spectra of  $K^+$  for each target nucleus and their characteristic features are presented. Also phenomenological fittings of the  $A$ -dependence of the  $(K^-, K^+)$  reaction in the form of  $A^n$  are explained. In sect 5, the data are confronted with some calculations. The measured momentum spectra are compared with a simple DWIA calculation with the eikonal method assuming only the quasifree processes,  $K^-(p) \rightarrow K^+\Xi^-$  and  $K^-(p) \rightarrow K^+\Xi^{*-}(1530)$ . A possible contribution on another reaction mechanism such as two-step processes is also mentioned. The conclusions are stated in sect. 6.

## 2. Experiment

The experiment was performed using the K2 beam line<sup>16)</sup> of the 12 GeV proton synchrotron at the National Laboratory for High Energy Physics (KEK). The experimental setup is shown in fig. 1. Since the details of the experimental equipments and their performances are described elsewhere<sup>17)</sup>, we give a brief description of the beam parameter, setup, trigger, targets and data acquisition system.

We use a separated  $K^-$  beam of which the momentum and momentum acceptance are 1.66 GeV/c and  $\pm 1\%$ , respectively. Typical value of the  $K^-/\pi^-$  ratio and the beam intensity are  $\frac{1}{3}$  and  $4.2 \times 10^3 K^-/\text{spill}$ . The beam particles are identified by using TOF counters (T1, T2) and an aerogel Čerenkov counter (AC1) which vetoes  $\pi^-$  in the beam. The TOF (T2-T1) resolution is 85 ps (r.m.s.), whereas the TOF difference between  $K^-$  and  $\pi^-$  is 850 psec. The refractive index of AC1 is 1.04 and the pion rejection efficiency is 99.3%. The  $\pi^-$  contamination in the  $K^-$  beam is, therefore, reduced to an order of  $10^{-6}$  in the final results.

The spectrometer consists of a magnet (0.7 T · m), silicon micro-strip detectors (BSSD, VSSD)<sup>18)</sup>, three sets of MWPCs (PC1-3) and MWDCs (DC1-3), an aerogel Čerenkov counter (AC2) and a TOF hodoscope (TOF). An outgoing particle is identified by the momentum measured with the tracking devices (VVSD, PC and DC) and the velocity deduced from the TOF and the track-length. The BSSD and VSSD, which are originally installed for the emulsion-counter hybrid experiment, have the position resolution of 16  $\mu\text{m}$  (r.m.s.) and they sandwich the target. The position resolution (rms) of the chambers are about 450  $\mu\text{m}$  for PC1, 210  $\mu\text{m}$  for DC1, 900  $\mu\text{m}$  for PC2-3 and 300  $\mu\text{m}$  for DC2-3. The momentum resolution of the spectrometer is 2.5% (r.m.s.) at 1.0 GeV/c. It is limited by the multiple scattering in the aerogel radiator (9.5 cm thick). The TOF of an outgoing particle is measured by the TOF hodoscope and T2. A TOF resolution of 85 ps (r.m.s.) is achieved, and it helps to make the spectrometer short to reduce the loss of  $K^+$  due to the in-flight decay. The mean path length of outgoing particles from the target to the TOF

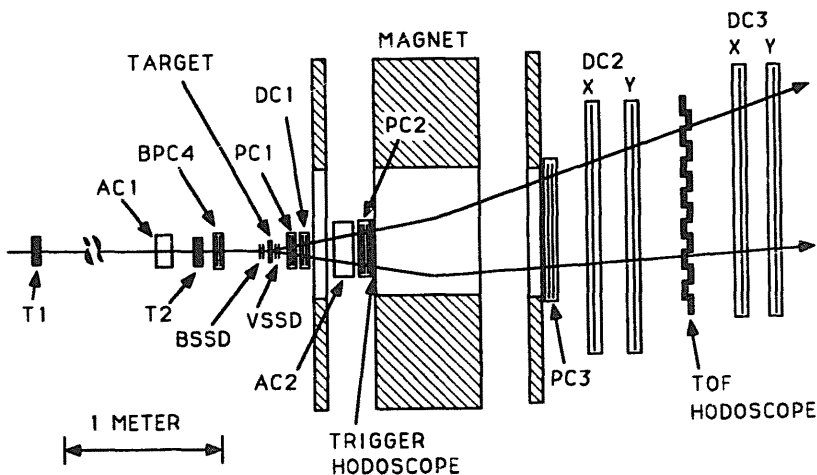


Fig. 1. Schematic view of the experimental setup.

hodoscope is about 2.8 m. The refractive index of AC2 is 1.06 and the pion rejection efficiency is 98.7% for 1.0 GeV/c pion. Performance of the identification of the outgoing particles is described in sect.3.

Because of the small cross section of the ( $K^-$ ,  $K^+$ ) reaction ( $\sim 35 \mu\text{b/sr}$  for proton target), the spectrometer is designed to have a large acceptance for positively charged particles. The acceptance is studied by a Monte Carlo simulation. It has a rectangular shape determined by the geometrical configuration of the experimental apparatus. Angular coverage for the outgoing particles is constant in vertical direction ( $|\theta_y| \leq 8.5^\circ$ ), while it varies according to the particle momentum  $p$  in horizontal direction ( $\theta_x$  ranges from  $\sim -14.5^\circ$  to  $\sim +10.5^\circ$  at  $p \sim 1.0 \text{ GeV/c}$  and it ranges from  $\sim -14.5^\circ$  to  $\sim +2.0^\circ$  at  $p \sim 0.5 \text{ GeV/c}$ ). The acceptance, therefore, has a dependence on the particle momentum  $p$  and its scattering angle  $\theta$ . The momentum dependence of the acceptance is shown in fig. 2. The acceptance is  $\sim 0.14 \text{ sr}$  at  $\sim 1.0 \text{ GeV/c}$  and falls down to a half of this value at  $\sim 0.45 \text{ GeV/c}$ . Since it is found in the off-line analysis that the outgoing particles (mainly protons) distribute almost uniformly in both vertical and horizontal directions, the acceptance can be estimated from the  $\theta_x$ - $\theta_y$  distribution of the particles in data. The momentum dependence of the acceptance estimated with this method is compared to the Monte Carlo simulation in fig. 2. They are consistent within 3%.

To reduce the trigger rate to an acceptable level, a trigger hodoscope (TH) and a scintillation counter (BV) are installed. The TH (8 elements) is used to form the  $8 \times 14$  matrix coincidence with the TOF hodoscope (14 elements) to identify the

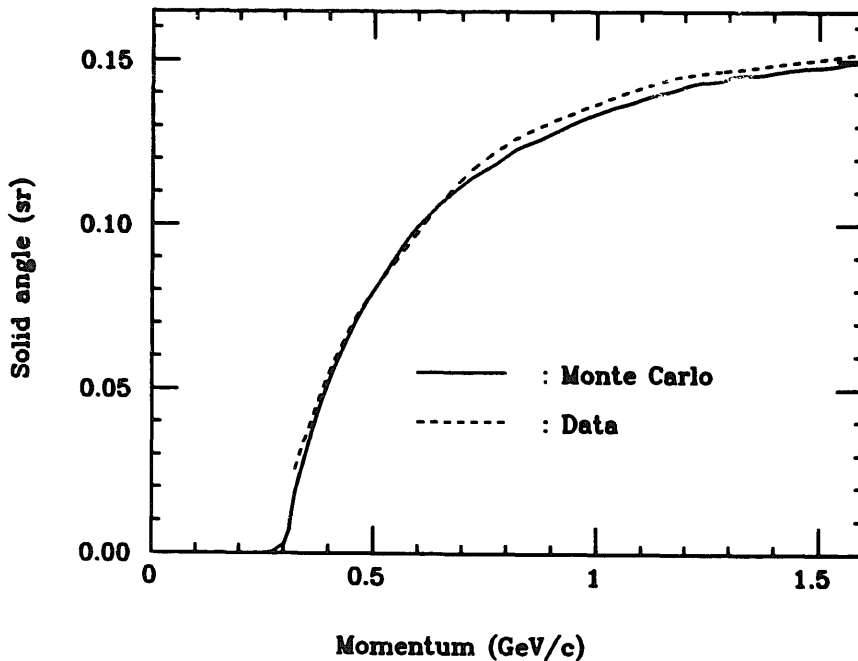


Fig. 2. Momentum dependence of the spectrometer acceptance. Solid line is the acceptance estimated by a Monte Carlo simulation. Dashed line is the one obtained from the actual distribution of the outgoing charged particles in data.

charge of the outgoing particle. The BV is used to kill the noninteracting beam particles. The on-line trigger is made by the logical product of  $T1 \otimes T2 \otimes \overline{AC1} \otimes \overline{AC2} \otimes \overline{BV} \otimes (+\text{charge})$ . But the  $\overline{AC2}$  is excluded from the on-line trigger for some runs to estimate the overkill of the ( $K^-$ ,  $K^+$ ) events associated with pions or electrons. An average trigger rate is 38 at  $4.2 \times 10^3 K^-/\text{spill}$ .

The targets used in the experiment are graphitic C (30 mm or 40 mm thick) and metal Al (30 mm thick), Cu (15 mm thick), Ag (15 mm thick) and Pb (15 mm thick). A polyethylene ( $C_nH_{2n}$ , 50 mm thick) target is also used for the measurement of the cross section with a hydrogen target. The carbon contribution is subtracted in the off-line analysis. Their thickness are chosen to be less than 0.1 interaction length. Due to the energy loss in the target, the  $K^-$  beam momentum at the center of the target is 1.65 GeV/c for each target. To avoid the systematic error in the A-dependence measurement coming from the run condition, the target species is alternated with a period of  $\sim 3$  hours during the run time which amounts to  $\sim 300$  hours in total.

Signals from the detectors are digitized by the standard CAMAC or KEK TKO <sup>19)</sup> modules. The output signals from the chambers are discriminated after an amplification and fed to the CAMAC latch modules (MWPCs) or TKO TDC modules (MWDCs). The amplified and shaped signals from BSSD and VSSD are digitized by 32 ch TKO ADC modules. The timing and pulse-height information from photomultipliers on TA, T2, AC1, AC2, BV, TH and TOF hodoscopes are read with CAMAC TDC and ADC. The digitized information is stored in the CAMAC memory buffer modules during the spill and then transferred to magnetic tapes after each spill. The CAMAC system is interfaced to a micro-VAX-2000 computer with a Kinetic 3922 crate controller.

### 3. Analysis

#### 3.1. SELECTION OF THE ( $K^-$ , $K^+$ ) EVENTS

At the on-line stage, the number of incident  $K^-$  is measured by using a scaler counting the coincidence events of the beam line TOF counters vetoed by the aerogel Čerenkov counter ( $T1 \otimes T2 \otimes \overline{AC1}$ ). In the off-line analysis, the TOF of beam particles is used to further reduce the contamination from other beam particles. From this off-line results and the on-line scaler readings, total numbers of the incident  $K^-$  are estimated to be 3.6, 1.3, 1.2, 2.7, 1.7 and  $4.1 \times 10^8$  for C, Al, Cu, Ag, Pb and  $CH_2$  targets, respectively.

To identify an outgoing particle, the mass of the particle is reconstructed by the momentum and the velocity which is deduced from the track length and TOF (TOF-T2). A particle trajectory is reconstructed by fitting the hit positions on tracking devices with a spline method <sup>20)</sup>. The ( $K^-$ ,  $K^+$ ) reaction is very rare compared to other processes such as ( $K^-$ ,  $\pi^+$ ) and ( $K^-$ , p) reactions. Moreover, there

are many background events due to the in-flight decays of non-interacting beam  $K^-$  and of elastically scattered  $K^-$  or  $K^+$  scattered by the materials such as aerogel blocks. The background rejection is, therefore, an important part of the analysis. The  $\pi^+$  contamination is reduced by requiring no signal from the aerogel Čerenkov counter (AC2). To reject the in-flight decay of beam  $K^-$ , we require the scattering angle of the outgoing particle at the target to be larger than  $1.7^\circ$ . The background due to the in-flight decay of the elastically scattered  $K^-$  and the  $K^-$  scattered by the materials can be reduced by requiring that the track has a small  $\chi^2$  value in the fitting.

The vertex of the reaction is reconstructed by using the hits on the tracking devices upstream and downstream of the target. Because of the good position resolution of the silicon micro strip detectors (BSSD and VSSD), the reaction vertex is beautifully reconstructed as shown in fig. 3. However the events which lack hits on BSSD or VSSD either due to the inefficiency or to the acceptance of the devices form the tail of the peak. We estimate the contamination of out of target events to be 3% in the selected region and that is mainly due to the reaction on BSSD or VSSD.

Fig. 4 shows the result of the particle identification.  $K^+$  is clearly identified. The events having the reconstructed mass between  $0.40$  and  $0.60 \text{ GeV}/c^2$  are selected as ( $K^-, K^+$ ) events. We estimate that the fraction of  $K^+$  out of this range is less than  $10^{-4}$  from the gaussian fitting of the peak shown in fig. 4 ( $\sigma = 26 \text{ MeV}/c^2$ ). The contamination of proton in the  $K^+$  mass region is estimated to be  $\sim 1\%$  from the fitting to the tail of the proton peak of an exponential curve shown also in the figure.

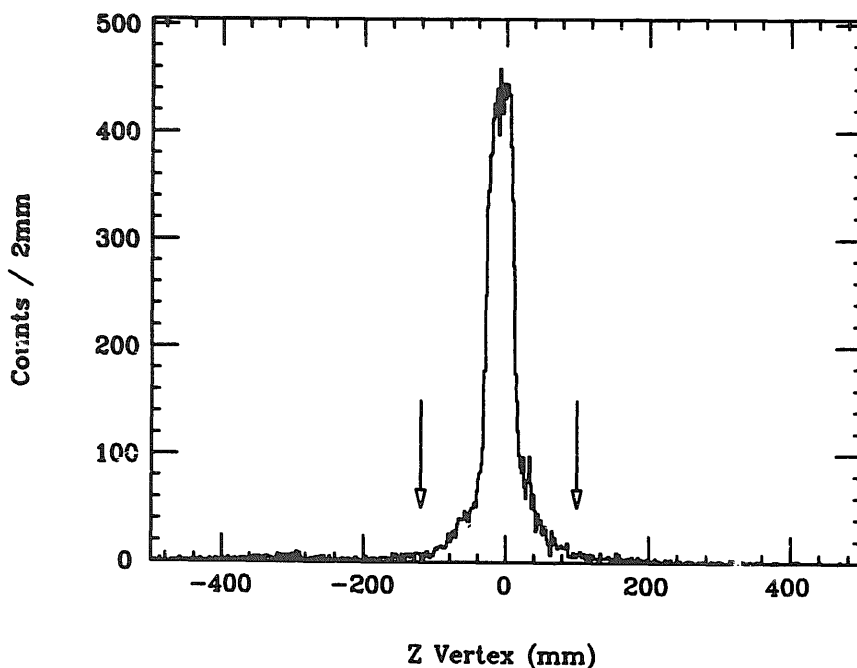


Fig. 3. Z-position of the reconstructed vertex (C-target, 40 mm thick). Arrows indicate the cut positions in the analysis.

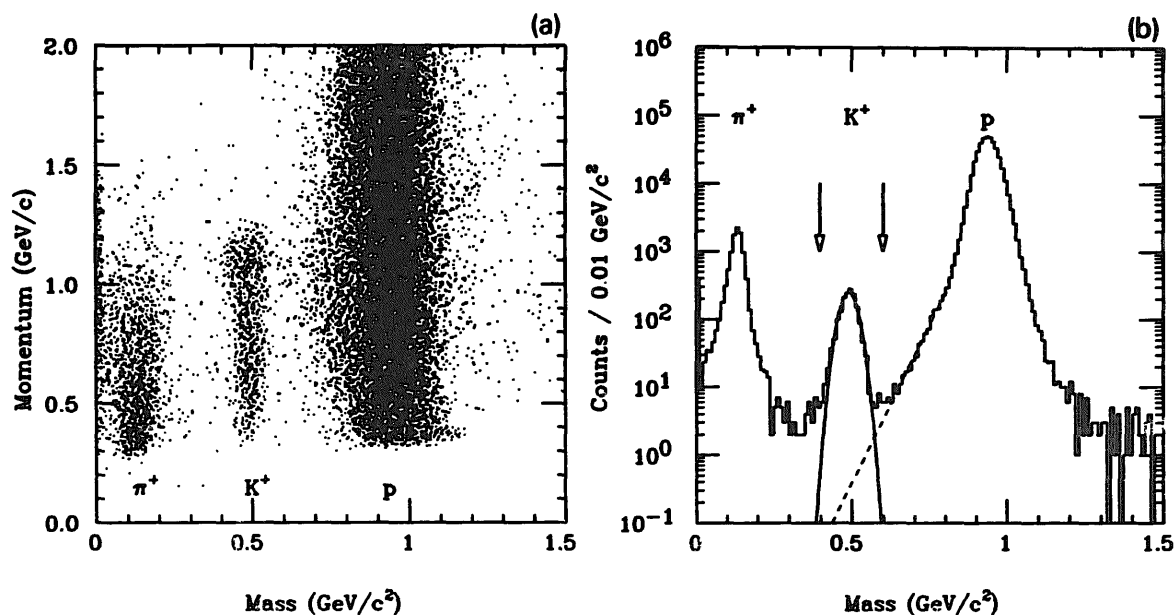


Fig. 4. (a) Measured momentum of the outgoing particle versus its reconstructed mass for the C-target. (b) Reconstructed mass of the particle which momentum is less than 1.3 GeV/c. Arrow indicate the criteria for the selection of ( $K^-$ ,  $K^+$ ) events. Solid curve is the fitted gaussian curve to the  $K^+$  peak ( $\sigma \sim 26$  MeV/c<sup>2</sup>). Dashed line shows the estimation of the proton contamination.

As for the contamination of  $\pi^+$ , we estimate it to be less than  $10^{-4}$  in all the momentum region below 1.3 GeV/c from the following reasons. From the data taken without AC2 in the on-line trigger, the number of  $\pi^+$  events is found to be about a hundred times larger than the  $K^+$  events. Since the mass difference between  $\pi^+$  and  $K^+$  corresponds to about 4 times the TOF resolution even at 1.3 GeV/c, the  $\pi^+$  contamination in that mass range is less than  $10^{-2}$  just with the TOF information. The  $\pi^+$  detection efficiency of AC2 is  $\sim 99\%$  in the momentum region above  $\sim 0.8$  GeV/c. Although it is less than 99% in the momentum region below  $\sim 0.8$  GeV/c, the mass difference corresponds to more than 10 times the TOF resolution in this momentum region.

After the event selection, the numbers of the reconstructed ( $K^-$ ,  $K^+$ ) events are about 1700 for C and CH<sub>2</sub>, 950 for Ag and 450 for Al, Cu and Pb targets. It should be noted that the events having the scattering angle  $\theta$  less than  $13.6^\circ$  are selected in order to present the cross section with a well-defined angular region.

### 3.2. DATA EVALUATION

The cross section is obtained as a function of the  $K^+$  momentum, taking the following corrections into account. First, a correction is made to the measured momentum of the outgoing  $K^+$  to take the energy loss in several materials between the target and the spectrometer (mainly the target itself and the AC2) into account. Secondly, the loss of  $K^+$  due to the in-flight decay ( $c\tau \sim 370.9$  cm) is corrected

according to the velocity and the flight-path length. Thirdly, the event is weighted with the spectrometer acceptance depending on the momentum and scattering angle of  $K^+$ . The result of the Monte Carlo simulation described in sect. 2 is used for this correction. Finally, the data is normalized to the number of incident  $K^-$ , taking into account (a) dead-time of the data acquisition, (b) tracking inefficiency which is determined by the inefficiencies of tracking devices and the tracking algorithm in the off-line analysis program, (c) overkill of the  $K^+$  by the off-line cuts and AC2 cut, (d) loss of the flux of  $K^-$  and  $K^+$  by the interaction in various materials and target and (e) contamination from the out of target events. Among these, (a) and the inefficiencies of tracking devices in (b) are measured for each run, and (c)–(e) are treated separately for each target. These values are estimated, on the average, to be (a) 12%, (b) 9%, (c) 22%, (d) 10% and (e) 3%.

Statistical uncertainty of the cross section is about  $\sim 3\text{--}6\%$  for the cross section integrated over all momentum region, according to the amount of data taken for each target. Systematic uncertainty is mainly due to the ambiguity in the estimations of the event reconstruction efficiency and of the fraction of  $K^+$  events killed by AC2. The error in the reconstruction efficiency depends on particle momentum. It is about  $\pm 2\%$  in the particle momentum region above  $0.5\text{ GeV}/c$ , while it is about  $\pm 5\%$  in the region below  $0.5\text{ GeV}/c$ . The  $K^+$  overkill by AC2 is caused by, for example, the energetic knock-on electrons produced in the aerogel blocks and the ( $K^-$ ,  $K^+$ ) reactions associated with pions. The normalization error for the integrated cross section is about  $\pm 6\%$  and it is mainly due to the ambiguity in the estimation of the  $K^+$  overkill by AC2.

## 4. Results

### 4.1. $K^+$ MOMENTUM SPECTRA

The obtained  $K^+$  momentum spectrum is shown in fig. 5 for each target nucleus. Also shown is the  $K^+$  momentum spectrum for proton target obtained by subtracting the carbon contribution from the spectrum for  $\text{CH}_2$  target. The spectra for nuclear targets (fig. 5a–e) are characterized by a peak at about  $1.1\text{ GeV}/c$  and a broad bump in the region below a dip at about  $0.95\text{ GeV}/c$ . Since the relative magnitude of the broad bump to the peak increases with the target mass number becomes larger, the dip is not so clear any more for Pb target.

The two peaks in the  $K^+$  spectrum for proton target (fig. 5f) are assigned to the two elementary processes;



The solid lines in fig. 5f show the positions and shapes of the peaks for these two processes simulated by a Monte Carlo calculation folding the momentum resolution of the spectrometer. The broadness of these peaks mainly comes from the kinematical

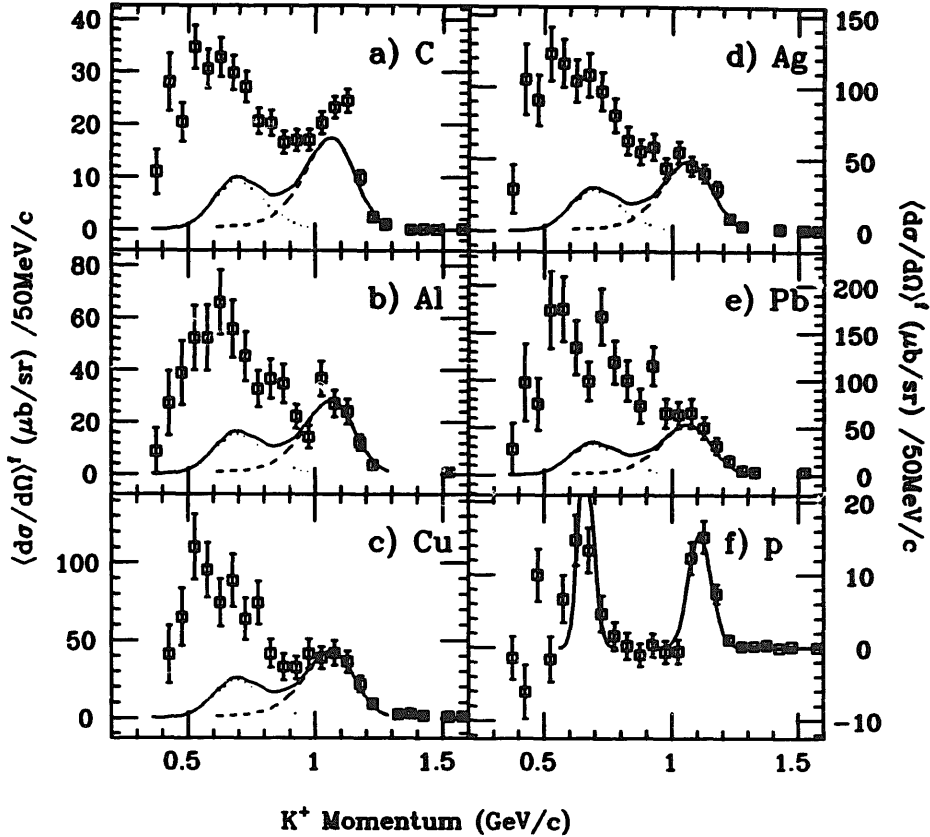


Fig. 5. Momentum spectra of  $K^+$  for target nucleus (a) C, (b) Al, (c) Cu, (d) Ag, (e) Pb. The spectrum for proton target, which is obtained from the subtraction of the C-contribution from  $\text{CH}_2$  target, is also shown in (f). Normalization error of the cross section is not included in the error bar. Solid, dashed and dotted curves in (a)-(e) are the calculated spectra for the  $K^-(p) \rightarrow K^+\Xi^-$  process (dashed),  $K^-(p) \rightarrow K^+\Xi^{*-}(1530)$  process (dotted) and some of these two (solid). See sect. 5.1.

effect due to the large acceptance. Cross sections for these cascade productions obtained for the data are as follows.

$$\begin{aligned} \langle d\sigma/d\Omega_L \rangle^f &= 35 \pm 4 \mu\text{b}/\text{sr} & \text{for } K^- + p \rightarrow K^+ + \Xi^-, \\ \langle d\sigma/d\Omega_L \rangle^f &= 40 \pm 7 \mu\text{b}/\text{sr} & \text{for } K^- + p \rightarrow K^+ + \Xi^{*-}(1530). \end{aligned}$$

Note that the cross section denoted by  $\langle d\sigma/d\Omega_L \rangle^f$  means the cross section averaged over the laboratory forward angular region between  $1.7^\circ$  and  $13.6^\circ$ , not the exact differential cross section at  $\theta_{\text{lab}} = 0^\circ$ . The uncertainties include the systematic errors as well as the statistical ones. The forward-angle cross section for the  $K^-p \rightarrow K^+\Xi^-$  reaction measured in the past experiments is summarized in ref. <sup>5)</sup> and the present result is consistent with the one measured at  $p_{K^-} = 1.60 \text{ GeV}/c$  by Berge *et al.* <sup>21)</sup>\*

The comparison of the  $K^+$  momentum spectrum for the nuclear target with that for the proton target indicates that the quasifree one-step processes;

$$K^- + (p) \rightarrow K^+ + \Xi^-, \quad K^- + (p) \rightarrow K^+ + \Xi^{*-}(1530),$$

\* As for the  $K^-p \rightarrow K^+\Xi^{*-}(1530)$  reaction, the total cross section measured by Berthon *et al.* at  $p_{K^-} = 1.65 \text{ GeV}/c$  is  $84 \pm 24 \mu\text{b}$ , but the angular distribution is not provided <sup>22)</sup>. If the angular distribution is isotropic in c.m., the laboratory forward cross section is  $d\sigma/d\Omega_L(0^\circ) = 69 \pm 20 \mu\text{b}/\text{sr}$ .

((p) means the proton in a nucleus) are the leading processes for the ( $K^-$ ,  $K^+$ ) reaction on nuclear targets at this energy. The peak at  $\sim 1.1$  GeV/ $c$  in the  $K^+$  momentum spectrum for every nuclear target (fig. 5a-f) is assigned to the peak due to the quasifree one-step process,  $K^-(p) \rightarrow K^+ \Xi^-$ , from its position and relatively narrow width, which is clearest in the spectrum for C-target. But the bump in the region below 0.95 GeV/ $c$  is too broad to be simply assigned to a smeared peak of the quasifree one-step process,  $K^-(p) \rightarrow K^+ \Xi^-(1530)$ . We discuss this point further in sect. 5.

#### 4.2. A-DEPENDENCE IN THE FORM OF $A^\alpha$

Since the whole structure of the quasifree peak around 1.1 GeV/ $c$  is not separated completely from the broad bump below 0.95 GeV/ $c$ , the  $A$ -dependence of the ( $K^-$ ,  $K^+$ ) reaction cross section is evaluated in two regions, above and below the dip at 0.95 GeV/ $c$ . In the present work, we call the region between 0.95 and 1.30 GeV/ $c$  "high momentum region" and the region between 0.35 and 0.95 GeV/ $c$  "low-momentum region". The cross sections integrated over these two regions and that over the whole region (0.35–1.30 GeV/ $c$ ) are tabulated for each target in table 1. As shown in fig. 6, they are well fitted by the form of  $CA^\alpha$ . The exponent  $\alpha$  is found to be  $0.38 \pm 0.03$  for the high-momentum region,  $0.56 \pm 0.02$  for the low-momentum region and  $0.52 \pm 0.02$  for the whole region. The constant  $C$  is  $37 \pm 4$   $\mu\text{b}/\text{sr}$ ,  $73 \pm 7$   $\mu\text{b}/\text{sr}$  and  $106 \pm 8$   $\mu\text{b}/\text{sr}$  for the respective regions. The reduced  $\chi^2$  for these fittings are 0.66, 0.48 and 0.31, respectively. Note that the measured cross sections for proton target plotted in the figure are not included in the fitting. For the high-momentum region, the extrapolation to  $A = 1$  of the fitted line falls very close to the cross section of the elementary process. This indicates that the single step quasifree process,  $K^-(p) \rightarrow K^+ \Xi^-$ , is dominant in this region. In addition, the fact that  $\alpha$  is close to  $\frac{1}{3}$  indicates that this quasifree process takes place mainly at

TABLE 1  
Integrated cross section ( $\mu\text{b}/\text{sr}$ )

Target	$K^+$ momentum region (GeV/ $c$ )				
	$0.95 < p_{K^+} < 1.30$		$0.35 < p_{K^+} < 0.95$		$0.35 < p_{K^+} < 1.30$
	data <sup>a)</sup>	(calc.) <sup>b)</sup>	data <sup>a)</sup>	(calc.) <sup>b)</sup>	data <sup>a)</sup>
C	$99 \pm 4$	(73)	$289 \pm 12$	(65)	$387 \pm 13$
Al	$118 \pm 11$	(117)	$472 \pm 35$	(107)	$590 \pm 37$
Cu	$190 \pm 17$	(178)	$719 \pm 50$	(166)	$908 \pm 53$
Ag	$226 \pm 15$	(201)	$1032 \pm 53$	(193)	$1259 \pm 55$
Pb	$296 \pm 30$	(224)	$1357 \pm 99$	(219)	$1653 \pm 103$

<sup>a)</sup> The normalization error ( $\pm 6\%$ ) is not included in the error.

<sup>b)</sup> The calculation is made with the DWIA method described in sect. 5.1.

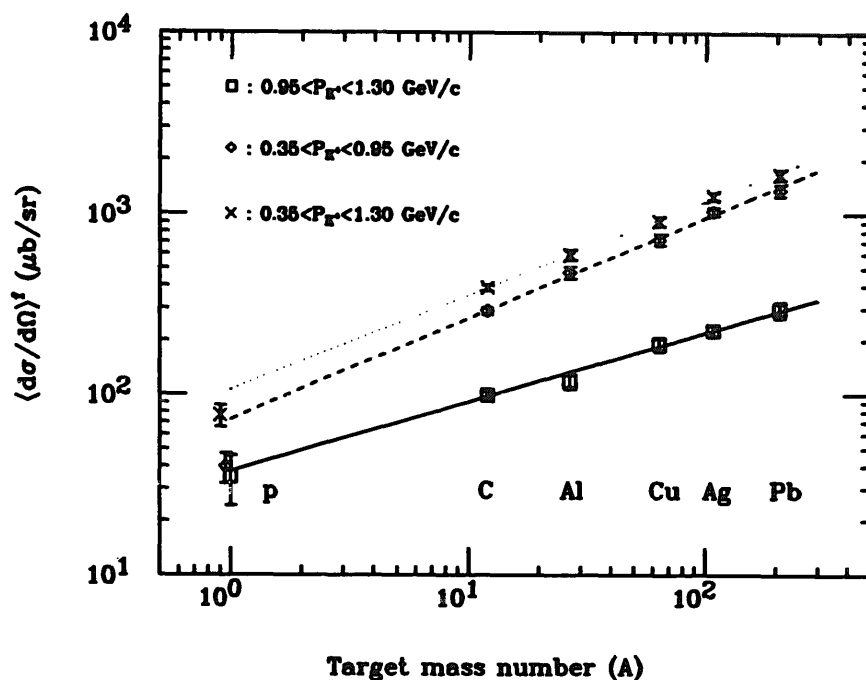


Fig. 6. Fitting of the  $A$ -dependence in the form of  $CA^n$ , for each  $K^+$  momentum region (solid:  $0.95 < p_K < 1.30$  GeV/ $c$ , dashed:  $0.35 < p_K < 0.95$  GeV/ $c$ , dotted:  $0.35 < p_K < 1.30$  GeV/ $c$ ). The measured cross sections for the proton target are also shown but they are not included in the fitting. The normalization error of the cross section is not included in the error bar.

the peripheral region of a target nucleus due to the absorption of incoming  $K^-$  or outgoing  $K^+$ . The cross section in the low-momentum region is characterized by its stronger  $A$ -dependence than in the high-momentum region. A further discussion on this point will be made in sect. 5.

## 5. Discussions

### 5.1. COMPARISON WITH DWIA CALCULATION

The obtained  $K^+$  momentum spectra are compared with a calculation based on the assumption that the reaction takes place via one-step quasifree processes,  $K^-(p) \rightarrow K^+ \Xi^-$  and  $K^-(p) \rightarrow K^+ \Xi^{*-}(1530)$ . In the present work, the  $K^+$  spectrum is simulated with a Monte Carlo method on the assumption that the reaction obeys the two-body kinematics between an incident  $K^-$  and a proton in a nucleus which has a Fermi type momentum distribution;

$$N(p) = N_0 / \left( 1 + \exp \left( \frac{p(\text{GeV}/c) - 0.1}{0.05} \right) \right).$$

The binding energy of the proton is taken to be 25 MeV. This momentum distribution was successfully used in the simulation of the  $K^+$  momentum spectrum for the quasifree process,  $K^-(p) \rightarrow K^+ \Xi^-$ , to reproduce the data for the emulsion target

measured separately with a higher statistics<sup>4</sup>). The fitting of the simulated spectrum to the quasifree peak is shown in fig. 7. The simulation is based on above momentum distribution and the ratio of the reactions on protons to those on nuclei in the emulsion target, which can be estimated from the  $A$ -dependence of the cross section in the high-momentum region described in sect. 4.1. Since our beam momentum is just above the threshold  $K^-$  momentum of  $K^-p \rightarrow K^+\Xi^{*-}$  (1530) process (1.51 GeV/c), it is important to take the energy dependence of the cross section carefully into account in the simulation. According to the data compiled in ref.<sup>8</sup>), we assume that the total cross section is 0 at  $E_{c.m.} \leq 2.04$  GeV/c, increases linearly with  $E_{c.m.}$ , and becomes constant at  $E_{c.m.} = 2.1$  GeV ( $E_{c.m.}$ ; center-of-mass energy of  $K^-p$ ). It is found that this energy dependence of the cross section affects the  $K^+$  momentum spectrum for this quasifree process significantly both in the shape and in the relative magnitude.

To compare the measured and calculated spectrum in an absolute scale, we calculate the cross section for the quasifree one step process with a DWIA method. In DWIA calculations, the laboratory forward-angle cross section on a nuclear target  $(d\sigma/d\Omega_L)|_A^0$  is expressed as

$$\frac{d\sigma}{d\Omega_L}|_A^0 = \frac{d\sigma}{d\Omega_L}|_p^0 \times Z_{\text{eff}},$$

where  $(d\sigma/d\Omega_L)|_p^0$  is the laboratory forward-angle cross section of the elementary process and  $Z_{\text{eff}}$  is the effective proton number which is calculated from the density distribution of a nucleus together with the distortion of incoming  $K^-$  and outgoing

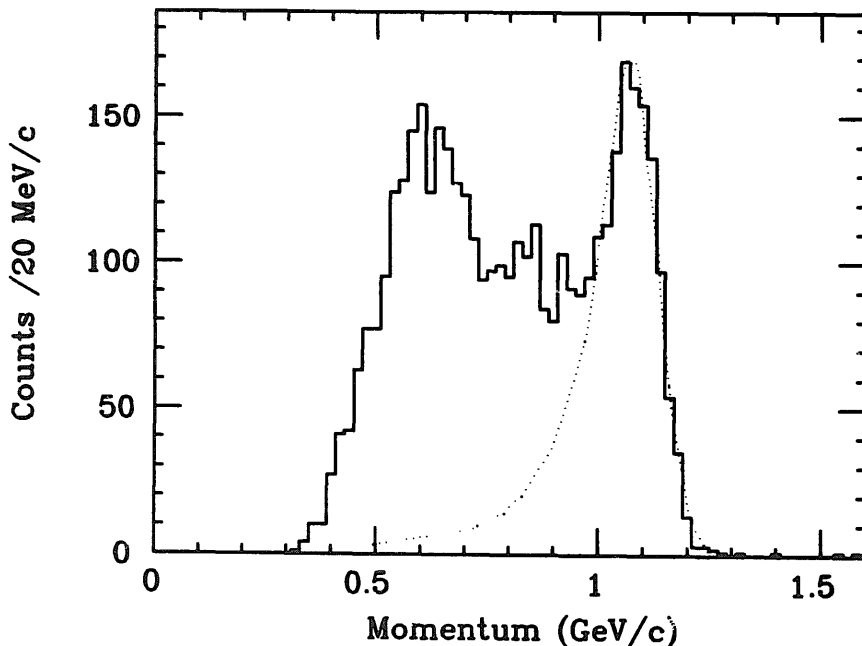


Fig. 7. Momentum spectrum of  $K^+$  measured separately for the emulsion target<sup>4</sup>). Dotted line is the calculated spectrum fitted to the peak. The calculation is based on the quasifree process  $K^-(p) \rightarrow K^+\Xi^-$ .

$K^+$  waves. With the eikonal approximation,  $Z_{\text{eff}}$  is expressed as <sup>24)</sup>

$$Z_{\text{eff}} = \frac{Z}{A} \int \rho(r) \exp \left[ -\bar{\sigma}_{K^-} \int_{-\infty}^z \rho(x, y, z') dz' - \bar{\sigma}_{K^+} \int_z^{\infty} \rho(x, y, z') dz' \right] dr.$$

In table 2,  $Z_{\text{eff}}$  for the two quasifree processes calculated by Bandō <sup>25)</sup> are listed for each target nucleus. In this calculation, the isospin-averaged total cross sections of  $K^\pm$  on a nucleon are taken to be  $\bar{\sigma}_{K^-} = 29.0$  mb,  $\bar{\sigma}_{K^+} = 18.4$  mb for  $K^-(p) \rightarrow K^+ \Xi^-$  and  $\bar{\sigma}_{K^+} = 13.3$  mb for  $K^-(p) \rightarrow K^+ \Xi^{*-}(1530)$ . The nuclear density distributions  $\rho(r)$  are quoted from ref. <sup>26)</sup>.

The calculated momentum spectra are compared with the measured spectra in the absolute scale in fig. 5a-e. In the figure, dashed and dotted curves correspond to the calculated spectrum for  $K^-(p) \rightarrow K^+ \Xi^-$  and  $K^-(p) \rightarrow K^+ \Xi^{*-}(1530)$ , respectively. The solid line is the sum of these two. The cross section for the elementary process used in this calculation is based on the present measurement (see sect. 4.1). Although the calculation underestimates the cross section for C-target by 26%, the good agreement between the measured and calculated spectrum in the high-momentum region indicates that the quasifree one step process,  $K^-(p) \rightarrow K^+ \Xi^-$ , is the dominant process in the high-momentum region. This is consistent with the fact that the shape of the quasifree peak for the emulsion target is reproduced fairly well by the simulated spectrum (fig. 7) and also with the result of the emulsion analysis where the  $\Xi^-$  tracks are observed in about 70% of the ( $K^-, K^+$ ) events in this momentum region <sup>3,4)</sup>. On the other hand, the measured spectra show an excess of the cross section compared to the calculation in the low-momentum region. In table 1 are listed the calculated cross sections integrated over the high- and low-momentum regions together with the measured ones. The measured cross sections are larger than the calculated ones by a factor of 4-6 in the low-momentum region.

## 5.2. CONTRIBUTION OF OTHER PROCESSES

Since the DWIA calculation based on one-step quasifree processes underestimates the cross section in the low-momentum region, the possible contribution of other processes is discussed.

TABLE 2  
Effective proton numbers  $Z_{\text{eff}}$  calculated with the DWIA method <sup>a)</sup>

Target	$K^-(p) \rightarrow K^+ \Xi^-$	$K^-(p) \rightarrow K^+ \Xi^{*-}(1530)$
<sup>12</sup> C	2.36	2.60
<sup>27</sup> Al	3.80	4.29
<sup>63</sup> Cu	5.77	6.76
<sup>107</sup> Ag	6.54	7.91
<sup>208</sup> Pb	7.27	9.05

<sup>a)</sup> The calculation is made by Bandō <sup>25)</sup>

At  $p_K = 1.65$  GeV/c, there are two more possible quasifree processes with three particles in the final state, namely  $K^-(p) \rightarrow K^+ \Xi^- \pi^0$  and  $K^-(p) \rightarrow K^+ \Xi^0 \pi^-$ . The threshold  $K^-$  momentum of these elementary processes is 1.34 GeV/c for both of them. According to ref. <sup>8)</sup> the total cross sections of their elementary processes at 1.65 GeV/c have been measured to be  $35 \pm 8 \mu\text{b}$  and  $20 \pm 6 \mu\text{b}$ , respectively. Dauber *et al.* <sup>23)</sup>, however, claimed that the decay from the  $K^+ \Xi^{*-}$  (1530) channel accounts for 64% and 51% of the  $K^+ \Xi^- \pi^0$  and  $K^+ \Xi^0 \pi^-$  channels, respectively. These are then less than 10% of the total cross section of  $K^- p \rightarrow K^+ \Xi^-$ , which is about  $150 \mu\text{b}$  [ref. <sup>8)</sup>]. Moreover, the measured  $K^+$  spectrum for the proton target (fig. 5f) does not show a broad peak which is characteristic of three-body reactions. We, therefore, conclude that the contribution of the three-body quasifree processes is small.

We need to investigate the possible contribution of higher-order process such as two-step processes. In these processes, two nucleons participate in the reaction. As described in sect. 4.2, the cross section in the low-momentum region has a larger  $A$ -dependence than in the high-momentum region. It is expected that the cross section due to a two-step process has a larger  $A$ -dependence than one-step process, because the number of nucleon pairs increases more rapidly than the nucleon number as the target mass number increases. Moreover, fig. 6 shows that the extrapolation of the fitted line to  $A = 1$  for the low-momentum region gives larger value than the measured cross section of the elementary process,  $K^- p \rightarrow K^+ \Xi^{*-}$  (1530). This fact indicates that the reaction channels which are open only for nuclear targets are important in the low-momentum region.

We focus the discussion on the two-step strangeness exchange reaction;



where  $N_1, N_2 = p$  or  $n$ ,  $\pi = \pi^0$  or  $\pi^\pm$  and  $Y_1, Y_2 = \Lambda, \Sigma$  or  $\Sigma^\pm$ . Any combination of  $N_1, N_2, \pi, Y_1$  and  $Y_2$  is allowed, if it conserves the charge. In a specific combination, the incident  $K^-$  has to find a  $N_1$  ( $=p$  or  $n$ ) out of the total  $A$  nucleons to produce the first reaction. The intermediate  $\pi$  has to find a  $N_2$  ( $=p$  or  $n$ ) out of the rest of  $A - 1$  nucleons to complete the reaction. The projected area of a nucleus varies as  $A^{2/3}$ . The cross section of a two step process, therefore, should be expressed as

$$\sigma \propto A^{2/3} \frac{Q_1 Q_2}{A(A-1)},$$

where  $Q_{1,2}$  is the number of available nucleons for each reaction ( $Q_1 Q_2 = Z(Z-1)$ ,  $ZN$  and  $N(N-1)$  for the respective combination of  $N_1$  and  $N_2$ , where  $Z$  is the number of protons and  $N$  is the number of neutrons in a nucleus). The  $A$ -dependence of the excess of cross section “ $\langle d\sigma/d\Omega \rangle_{\text{excess}}$ ”, which is defined by

$$\langle d\sigma/d\Omega \rangle_{\text{excess}} = \langle d\sigma/d\Omega \rangle_{0.35-0.95}^{\text{exp}} - \langle d\sigma/d\Omega \rangle_{0.35-0.95}^{\text{DWIA}},$$

is compared with this simple model. In this definition,  $\langle d\sigma/d\Omega \rangle_{0.35-0.95}^{\text{exp}}$  is the measured integrated cross sections in the low momentum region and  $\langle d\sigma/d\Omega \rangle_{0.35-0.95}^{\text{DWIA}}$

is the one calculated with the DWIA method (table 1). In fig. 8, is shown the ratio  $R$ ;

$$R = \frac{\langle d\sigma/d\Omega \rangle_{\text{excess}}}{A^{2/3} Q_1 Q_2 / (A(A-1))}$$

for three combinations of  $Q_1 Q_2$  as (a)  $Z(Z-1)$ , (b)  $ZN$  and (c)  $N(N-1)$ . As shown in the figure, the ratio  $R$  is almost constant for the five targets for  $N_{1,2} = pp$  or  $pn$ . Therefore, the  $A$ -dependence of the  $\langle d\sigma/d\Omega \rangle_{\text{excess}}$  is consistent with this model. The ratio  $R$  is, however, not constant for  $N_{1,2} = nn$ . It is reasonably understandable that the process  $N_{1,2} = nn$  should be suppressed in a double charge exchange reaction. These results indicate that the contribution of two-step processes is significant in the low-momentum region.

The cross sections of several two-step processes are roughly evaluated at  $p_K = 1.65 \text{ GeV}/c$ , following the method that Dover described in ref. <sup>13</sup>). Using the cross sections of the two elementary process  $[d\sigma/d\Omega]_{1,2}^{0^\circ}$ , the forward-angle differential

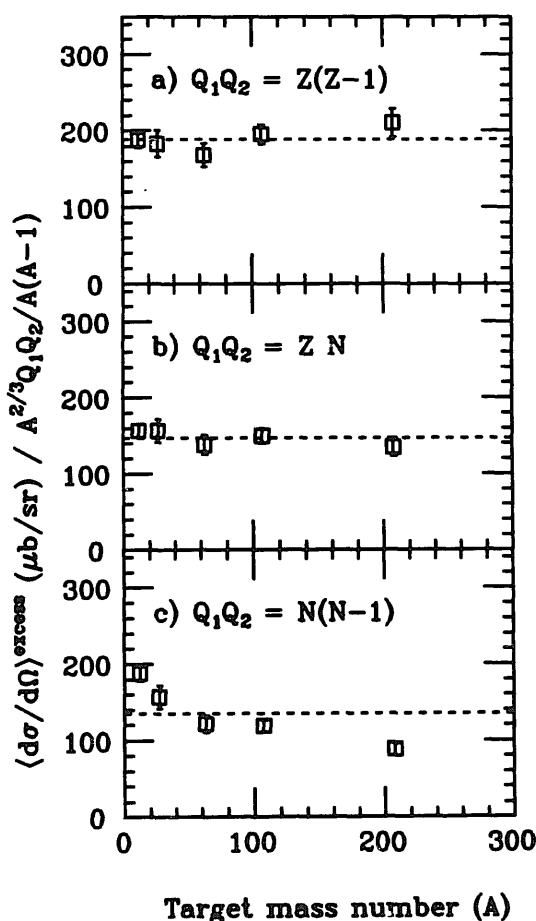


Fig. 8. Excess of the measured cross section over the DWIA calculation ( $\langle d\sigma/d\Omega \rangle_{\text{excess}}$ ), integrated over the low momentum region ( $0.35 < p_K < 0.95 \text{ GeV}/c$ ). They are normalized by  $A^{2/3} Q_1 Q_2 / A(A-1)$  where (a)  $Q_1 Q_2 = Z(Z-1)$ , (b)  $Q_1 Q_2 = ZN$  and (c)  $Q_1 Q_2 = N(N-1)$ . Dashed line in each figure shows the average of the ratio  $R$  for five targets.

cross section summed over all final states for one nucleon pair is given by

$$\sum_r \left[ \frac{\sigma}{d\Omega_L} \right]_r^{0^0} \approx \frac{2\pi\alpha_1\alpha_2\xi}{p_\pi^2} \left\langle \frac{1}{r^2} \right\rangle \left[ \frac{d\sigma}{d\Omega_L} \right]_1^{0^0} \left[ \frac{d\sigma}{d\Omega_L} \right]_2^{0^0},$$

where  $\xi$  is the characteristic of the angular distribution of the two elementary processes,  $\langle 1/r^2 \rangle$  is the mean inverse-square radial separation of the proton pair,  $p_\pi$  is the laboratory pion momentum and  $\alpha_{1,2}$  is the kinematical factor which relates the  $t$ -matrix to the forward-angle laboratory cross section for each process\*. In table 3 are listed the calculated cross sections  $\sum_r [d\sigma/d\Omega_L]_r^{0^0}$  for several processes for which the elementary cross section  $[d\sigma/d\Omega_L]_{1,2}^{0^0}$  and  $\xi$  can be estimated based on the data given by the past experiments<sup>27)</sup> and charge independence. The cross section for a nucleus is obtained by multiplying the cross section for one nucleon pair by an "effective number of nucleon pair". If we neglect the distortion of mesons, they are  $Z(Z-1)$ ,  $ZN$  or  $N(N-1)$  for the respective combination of  $N_1$  and  $N_2$ . In the case of the C-target, the rough estimation yields about  $16 \mu\text{b/sr}$  in total of the processes listed in table 3.

TABLE 3  
Calculated cross sections of the two-step processes  
 $\sum_r [d\sigma/d\Omega_L]_r^{0^0}$  for one nucleon pair

Process 1	Process 2	$\sum_r \left[ \frac{d\sigma}{d\Omega_L} \right]_r^{0^0}$ ( $\mu\text{b/sr}$ )
$K^- p \rightarrow \pi^0 \Lambda$	$\pi^0 p \rightarrow K^+ \Lambda$	0.08
$K^- p \rightarrow \pi^+ \Sigma^-$	$\pi^+ p \rightarrow K^+ \Sigma^+$	0.12
$K^- p \rightarrow \pi^- \Sigma^+$	$\pi^- p \rightarrow K^+ \Sigma^-$	0.02
$K^- p \rightarrow \pi^0 \Lambda$	$\pi^0 p \rightarrow K^+ \Sigma^0$	0.06
$K^- p \rightarrow \pi^0 \Lambda$	$\pi^0 n \rightarrow K^+ \Sigma^-$	0.05
$K^- p \rightarrow \pi^+ \Sigma^-$	$\pi^+ n \rightarrow K^+ \Lambda$	0.10
$K^- n \rightarrow \pi^- \Lambda$	$\pi^- p \rightarrow K^+ \Sigma^-$	0.02
$K^- p \rightarrow \pi^+ \Sigma^-$	$\pi^+ n \rightarrow K^+ \Sigma^0$	0.04

This is an order of magnitude smaller than the observed value. However, there are seven more possible processes which have  $K^- p \rightarrow \pi^0 \Sigma^0$ ,  $K^- n \rightarrow \pi^- \Sigma^0$  or  $K^- n \rightarrow \pi^- \Sigma^0$  as the first reaction even in this category of the two-step process. If  $\Sigma^*(1385)$  and  $\Lambda^*(1405)$  productions are included, the number of possible two-step process becomes 45. Moreover, there can be two-step processes which have  $\eta$ ,  $\rho$  or  $\omega$  meson as an intermediate meson. The estimation for these processes is not possible partly because of the lack of data for these elementary processes. Therefore, further experimental and theoretical efforts are needed for a better understanding about the two step process in the ( $K^-$ ,  $K^+$ ) reaction.

\* Eq. 14 in ref. 13) is not correct. It should be divided by  $4\pi$ ; C. Dover, private communication.

## 6. Conclusion

The forward-angle cross sections of the double strangeness and double charge exchange ( $K^-$ ,  $K^+$ ) reaction on C, Al, Cu, Ag and Pb nuclei are measured for the first time. The incident  $K^-$  momentum is 1.65 GeV/*c*. The measured  $K^+$  momentum spectrum for each target nucleus is characterized by a quasifree peak in the  $K^+$  momentum region above 0.95 GeV/*c* and a broad bump in the region below 0.95 GeV/*c*. A comparison of the measured spectrum with a DWIA calculation is made on the assumption that the reaction proceeds via quasifree one step processes,  $K^-(p) \rightarrow K^+ \Xi^-$  and  $K^-(p) \rightarrow K^+ \Xi^{*-}(1530)$ . The good agreement between the measured and calculated spectrum in the high  $K^+$  momentum region indicates that the quasifree one-step process is dominant in this momentum region. In addition, the *A*-dependence of the cross section in the high-momentum region ( $A^{0.38 \pm 0.03}$ ) indicates that this quasifree process takes place at the peripheral of the target nucleus. On the other hand, the cross section of the bump in the low  $K^+$  momentum region is larger than the DWIA calculation by a factor of 4–6, and it has a larger *A*-dependence ( $A^{0.56 \pm 0.02}$ ) than in the high-momentum region. The *A*-dependence of the excess of the measured cross section over the DWIA calculation is explained by the simple model of two-step process which indicates that the two step strangeness exchange reactions,  $K^- N_1 \rightarrow \pi Y_1$  followed by  $\pi N_2 \rightarrow K^+ Y_2$ , have an important contribution in the low momentum region. For a better understanding of the reaction mechanism in this region, further theoretical and experimental efforts are needed.

We would like to express our thanks to the staff of KEK for their support to the experiment. We thank Professors H. Sugawara, K. Nakai and K. Takamatsu for their continuous encouragement throughout this work. We gratefully acknowledge late Professor H. Bandō for the helpful discussions on the calculation and the advice on the experiment. It was our great regret that he passed away in January 1990. We also appreciate the cooperation of the E176 collaborators in the execution of the experiment. This experiment was supported in part by a Grant-in-Aid for Scientific Research, the Ministry of Science, Culture and Education in Japan and the Basic Science Research Institute program.

## References

- 1) A.T.M. Aerts and C.B. Dover, Phys. Rev. **D29** (1984) 433
- 2) D. Zhu, C.B. Dover, A. Gal and M. May, Phys. Rev. Lett. **67** (1991) 2268
- 3) S. Aoki *et al.*, Prog. Theor. Phys. **85** (1991) 1287
- 4) S. Aoki *et al.*, Prog. Theor. Phys. **85** (1991) 951
- 5) A.T.M. Aerts and C.B. Dover, Phys. Rev. **D28** (1983) 450
- 6) C.B. Dover and A. Gal, Ann. of Phys. **146** (1983) 309
- 7) S. Aoki *et al.*, Phys. Rev. Lett. **65** (1990) 1729
- 8) V. Flaminio, W.G. Moorhead, D.R.O. Morrison and N. Rivoire, CERN-HERA Report 83-02 (1983)
- 9) G. d'Agostini *et al.*, Nucl. Phys. **B209** (1982) 1
- 10) R. Bertini *et al.*, Nucl. Phys. **A360** (1981) 315

- 11) A. Bouyssy Nucl. Phys. **A290** (1977) 324
- 12) A. Bouyssy, Phys. Lett. **B99** (1981) 373
- 13) C.B. Dover, Nukleonika **25** (1980) 521
- 14) A.J. Baltz, C.B. Dover and D.J. Millener, Phys. Lett. **B123** (1983) 9
- 15) P.A.M. Gram *et al.*, Phys. Rev. Lett. **62** (1989) 1837
- 16) A. Yamamoto *et al.*, Nucl. Instr. Meth. **203** (1982) 35
- 17) S. Aoki *et al.*, to be published
- 18) H. Tajima, S. Nakanishi, M. Nakamura, K. Niwa, H. Tanaka and K. Yamamoto, Nucl. Instr. Meth. **A288** (1990) 536
- 19) T.K. Ohsuka *et al.*, KEK report 85-10 (1985)
- 20) H. Wind, Nucl. Instr. Meth. **115** (1974) 431
- 21) J.P. Berge *et al.*, Phys. Rev. **147** (1966) 945
- 22) A. Berthon *et al.*, Nuovo Cim. **A21** (1974) 154
- 23) P.M. Dauber *et al.*, Phys. Rev. **179** (1969) 1262
- 24) H. Bandō, T. Motoba and J. Žofka, Int. J. Mod. Phys. **A5** (1990) 4021
- 25) H. Bandō, private communication, 1989
- 26) C.W. DeJager, H. De Vries and C. De Vries, At. Data Nucl. Data Tables **14** (1974) 479
- 27) A. Berthon *et al.*, Nucl. Phys. **B20** (1970) 476;  
D.F. Kane Jr., Phys. Rev. **D5** (1972) 1583;  
D.H. Saxon *et al.*, Nucl. Phys. **B162** (1980) 522;  
O.I. Dahl, L.H. Hardy, R.I. Hess, J. Kirz, D.H. Miller and J.A. Schwartz, Phys. Rev. **163** (1967) 1430  
M. Winnik, S. Toaff, D. Revel, J. Goldberg and L. Berny, Nucl. Phys. **B128** (1977) 66;  
J.C. Hart *et al.*, Nucl. Phys. **166** (1980) 73